ACS MATERIALS LETTERS

www.acsmaterialsletters.org

Toward the Development of a High-Voltage Mg Cathode Using a Chromium Sulfide Host

Lauren Blanc,[#] Christopher J. Bartel,[#] Haegyeom Kim, Yaosen Tian, Hyunchul Kim, Akira Miura, Gerbrand Ceder,[*] and Linda F. Nazar[*]

Cite This: *ACS Materials Lett.* 2021, 3, 1213–1220

Read Online

ACCESS | Metrics & More | Article Recommendations | Supporting Information

ABSTRACT: **Development of Mg-ion batteries as advanced electrochemical energy storage systems relies on the design and discovery of high-voltage positive electrode (cathode) materials. To date, a variety of sulfide cathodes have been reported (e.g., $Mg_xMo_6S_8$, $Mg_xTi_2S_4$, etc.), but the voltages of these materials are too low to prepare a high energy density Mg cell. Theoretical computations predicted that $Mg_xCr_2S_4$ operating with the high-voltage $Cr^{3+/4+}$ redox couple would serve as a suitable cathode candidate, but experimental attempts to extract Mg^{2+} from the lattice have been largely unsuccessful. We show that reversible electrochemical activity within a thiospinel framework (AB_2S_4) relies on a redox-active transition metal present in the *B* site; otherwise, anionic redox activity triggers decomposition of the spinel structure. Since Cr and S states are highly coupled in $MgCr_2S_4$, the $Cr^{3+/4+}$ redox couple is inaccessible so that reversible (de)intercalation of Mg^{2+} cannot occur and charging leads to dissolution of the active material. These findings point to an insufficiency in the screening criteria previously used to identify $MgCr_2S_4$ as a promising Mg cathode. Thus, a computable descriptor based on the electronic structure of the discharged material is proposed to predict the prevalence of cation vs anion redox and improve future surveys of potential candidates. It is unlikely that the high-voltage Cr redox couple will be accessible to oxidation in the presence of sulfur within the restrictions of a spinel framework; however, it is possible that a suitable layered Mg_xCrS_2 structure could serve as a reversible high-voltage Mg cathode.**

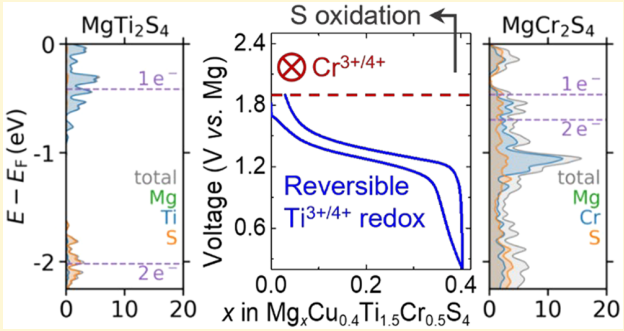

Intensifying environmental concerns demand a transition from gasoline-powered cars and excessive fossil fuel consumption toward sustainable practices and widespread utilization of renewable resources such as wind and solar. However, to successfully increase the number of electric vehicles on the road and integrate intermittent power sources into the grid, affordable electrochemical energy storage systems must still be developed.[1,2] While lithium ion batteries (LIBs) are currently the dominant choice for electrochemical energy storage, safety concerns and possible rising costs of this technology have driven the search for alternative approaches.[3−5] Magnesium ion batteries (MIBs) have garnered considerable recognition as promising candidates.[6−10] As a geologically abundant element (eighth-most abundant element in Earth's crust and second-most abundant metal ion in seawater), magnesium metal is widely available and more affordable than the scarce resources employed in commercial lithium cells. Furthermore, Mg-based technology has the potential to provide increased energy density beyond the theoretical limitations of lithium batteries owing to Mg's low reduction potential (−2.37 V vs SHE) and the exceptionally high volumetric capacity of the metal (3832 mAh·cm^{-3}). Finally, MIBs offer superior safety relative to Li-based systems because Mg metal is stable in ambient conditions and—depending on the current density and electrolyte used—Mg negative electrodes (anodes) can be resistant to dendritic electrodeposition that would otherwise penetrate separators and short circuit cells.[11,12]

Despite these benefits, there are several challenges plaguing the development of MIBs and similar multivalent systems based on Zn, Ca, and other abundant metals. Positive electrode (cathode) selection is severely restricted by the strong electrostatic attractions between divalent ions and their surrounding anions which leads to sluggish solid-state diffusion and a strong tendency toward competing conversion

Received: May 25, 2021
Accepted: June 29, 2021
Published: July 15, 2021

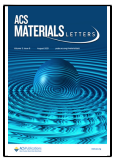

https://doi.org/10.1021/acsmaterialslett.1c00308
ACS Materials Lett. 2021, 3, 1213–1220

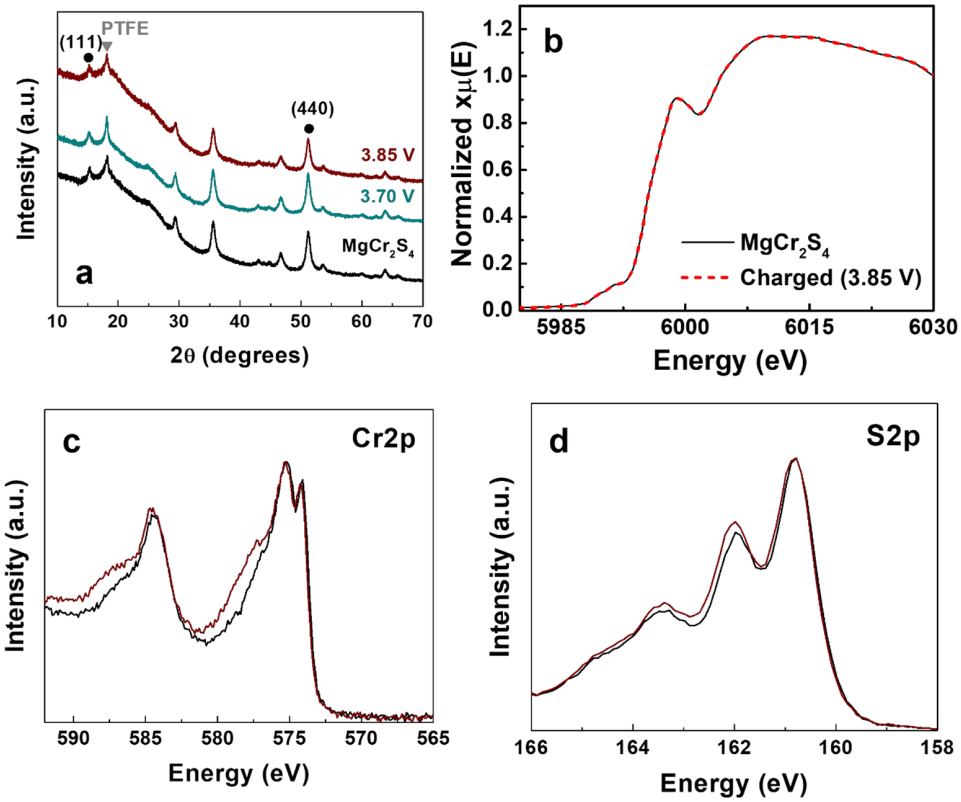

Figure 1. Ex situ analysis of pristine $MgCr_2S_4$ and charged material: (a) XRD patterns, (b) XANES spectra, and XPS spectra of (c) Cr 2p and (d) S 2p edges showing $MgCr_2S_4$ (black) and material charged to 3.85 V (brown).

mechanisms.[13−15] In electrolyte solution, desolvation penalties slow (de)intercalation kinetics and complicate interfacial interactions that can trigger electrolyte decomposition and passivate electrode surface(s).[16−18] As a result, most well-known transition metal oxide hosts employed in Li-ion cells cannot serve as cathodes in MIBs, and alternative platforms must be explored.[19] A promising strategy to circumvent the kinetic impediments of highly polarizing oxides is to instead develop sulfide-based cathode materials. The relatively "soft" nature of sulfides (compared to oxides) leads to weaker interactions with migrating Mg^{2+} cations, enabling reversible electrochemical activity.[20] Indeed, the first successful demonstration of a rechargeable MIB by Aurbach et al. paired a Chevrel phase Mo_6S_8 cathode vs Mg metal.[21] Since this seminal work, reversible Mg^{2+} storage operating on intercalation chemistry has been demonstrated in a variety of sulfide hosts.[22−24]

Among potential sulfide candidates, robust thiospinel frameworks belonging to the cubic $Fd\bar{3}m$ space group (227) are of particular interest because of their phase stability and high intrinsic electronic conductivity.[25,26] Spinel compounds have the general formula AB_2X_4 where B cations are octahedrally coordinated by chalcogenide X anions (e.g., O^{2-}, S^{2-}, Se^{2-}, etc.). Edge-sharing BX_6 octahedra create a three-dimensional network of diffusion channels in which A cations typically occupy tetrahedrally coordinated sites. Thus far, our group has demonstrated two thiospinel frameworks as successful hosts capable of reversible Mg^{2+} intercalation with high capacities and reasonably long cycle lives: $Mg_xTi_2S_4$ and $Mg_xZr_2S_4$, which store up to 0.8 mol of Mg^{2+} at operating voltages of 1.2 and 0.8 V vs Mg, respectively.[22,24] While these candidates offer an excellent platform to investigate fundamental aspects of Mg^{2+} intercalation, their operating voltages are too low to prepare a high energy density Mg cell. Higher voltages can be achieved in oxide spinel frameworks, but these materials can suffer from low capacities and poor reversibility due to sluggish kinetics and potential spinel to rock-salt conversion processes at the electrode surface.[27,28] In the search for alternative Mg thiospinel cathodes, computational screening identified $MgCr_2S_4$ as a promising candidate.[20] Benefiting from the high voltage $Cr^{3+/4+}$ redox couple, $MgCr_2S_4$ offers several attractive properties as a Mg cathode, including a high gravimetric energy density of 345 $Wh{\cdot}kg^{-1}$ and a relatively low (calculated) Mg^{2+} migration barrier of 540 meV. Despite these desirable metrics, successful $MgCr_2S_4$ electrochemsitry has yet to be demonstrated.

A $Mg_xCr_2S_4$ active material can be electrochemically evaluated starting with either (1) Mg^{2+} extraction from magnesiated materials or (2) Mg^{2+} insertion into host materials. $MgCr_2S_4$ can be prepared by a direct solid-state reaction or metathesis reactions,[29,30] or the thiospinel host can be synthesized with a different metal in the A site (e.g., Cu) and then chemically oxidized to remove that sacrificial A site, leaving available sites for Mg^{2+} insertion on discharge. In this work, we explore both methods of preparing the active material to evaluate and compare electrochemical performance. In addition to nanosized $MgCr_2S_4$, we also prepared and investigated a $CuTi_xCr_{2-x}S_4$ solid solution series to evaluate how the extent of metal extraction from the spinel A site varies as a function of the transition metal(s) present on the B site. Finally, we employ computational methods to explore the electronic structure of MgM_2S_4 (M = Ti, V, Cr) thiospinels to

https://doi.org/10.1021/acsmaterialslett.1c00308
ACS Materials Lett. 2021, 3, 1213−1220

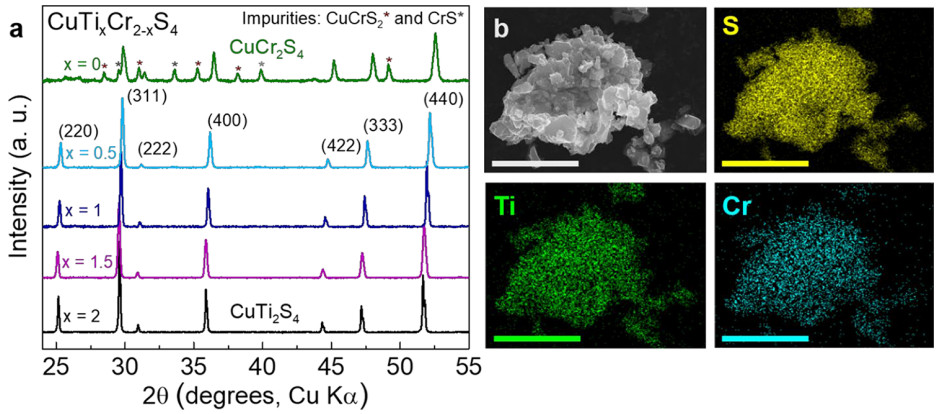

Figure 2. (a) XRD patterns of $CuTi_xCr_{2-x}S_4$. Impurities are observed in $CuCr_2S_4$ but materials containing Ti show a single phase thiospinel. (b) Elemental mapping of $CuTi_{1.5}Cr_{0.5}S_4$ where each scale bar represents 5 μm.

identify intrinsic properties impacting their electrochemistry. The theoretical analysis used here provides a useful approach to rapidly screen future materials for their propensity to undergo cation/anion redox.

Traditionally, the preparation of phase-pure $MgCr_2S_4$ has posed significant challenges to synthetic chemists owing to the slow kinetics of consuming Cr_2S_3. Wustrow et al. showed that excess MgS precursor can promote complete reaction of Cr_2S_3 at 800 °C, but a subsequent acid wash was needed to obtain the targeted $MgCr_2S_4$ product.[29] After this preparation, solid-state $MgCr_2S_4$ showed no significant charge capacity in a variety of electrolytes, but this poor performance could be due to surface degradation of the active material as a result of the harsh acid treatment and/or kinetic challenges due to the large particle size of the material resulting from long high temperature heat treatments. Because crystallite size is known to have a significant impact on the electrochemical performance of sulfide-based Mg cathode materials,[31] we investigated the electrochemistry of nanosized $MgCr_2S_4$ prepared using a recently reported metathesis synthesis (Figure S1).[30] This metathesis method of preparation benefits from a rapid, low temperature synthetic route achievable due to the strong thermodynamic driving force of NaCl formation (eq 1), which can easily be removed by washing with water.

$$MgCl_2 + 2NaCrS_2 \rightarrow MgCr_2S_4 + 2NaCl \quad (1)$$

Electrodes were prepared with these nanosized $MgCr_2S_4$ platelets and then charged in a Li cell to high voltage, up to 3.85 V vs Li which corresponds to 3.2 V vs Mg, to attempt Mg^{2+} extraction. Unlike previous reports that showed capacities less than 10 mAh·g^{-1} on electrochemical oxidation,[29] a significant charge capacity of 76 mAh·g^{-1} was observed in this Li cell, which could correspond to 0.37 mol of Mg^{2+} removed (Figure S2). Therefore, a variety of characterization methods were employed to explore the extent of demagnesiation (Figure 1).

Figure 1a shows the diffraction patterns of pristine $MgCr_2S_4$ as well as material charged to 3.70 and 3.85 V vs Li (3.05 and 3.2 V vs Mg, respectively) in a Li cell. The broadness of the peaks associated with the marked thiospinel reflections is indicative of the nanosized crystallites of the active material. Successful Mg^{2+} extraction should be accompanied by contraction of the thiospinel structure, which would correspond to a right-ward shift of these spinel reflections. In addition, the intensity ratio (111)/(440) should change significantly if some Mg^{2+} is extracted from $Mg_xCr_2S_4$. However, no changes in XRD peak positions and/or intensity ratios are observed, suggesting the cathode material remains fully (or nearly fully) magnesiated. This conclusion is further supported by overlapping XANES spectra of the pristine and charged material (Figure 1b), indicating that Cr^{3+} has not been oxidized to Cr^{4+}, again suggesting limited or no Mg^{2+} removal. While no redox activity was evident in bulk material from XANES analysis, the surface-sensitive XPS shows a slight shift to higher binding energies in both Cr and S 2p signals (Figure 1c, d). We conclude that electrochemical oxidation was restricted to the surface of $MgCr_2S_4$ particles with no significant Mg^{2+} extraction from bulk electrode material. Post-mortem analysis of the cell showed the presence of black material on the charged separator, and EDX elemental analysis confirmed that this deposit contains both Cr and S (Figure S3). This observation suggests that the competing anionic redox activity taking place during charge of $MgCr_2S_4$ destabilizes the spinel framework such that Mg^{2+} extraction is accompanied by the formation of sulfide holes, which leads to the dissolution of active material from the electrode.

Since reversible redox activity could not be achieved with $MgCr_2S_4$ cathode material, the Cr thiospinel was prepared with Cu in the A site, akin to the methodology used to prepare Ti_2S_4 and Zr_2S_4 electrodes,[22,24] to evaluate how much Mg^{2+} can be extracted depending on transition metal(s) present on the B site. The preparation of $CuCr_2S_4$ is challenged by competition with the thermodynamically favored $CuCrS_2$ layered phase. However, partial substitution of Ti in the spinel *B* site allows for the formation of the phase-pure thiospinel, and a solid solution series forms with varying Ti content (Figure 2). $CuTi_xCr_{2-x}S_4$ samples that contain at least $x = 0.5$ Ti only show reflections corresponding to the cubic $Fd\bar{3}m$ spinel phase whereas samples with no Ti ($x = 0$) contain a variety of Cu and/or Cr sulfide impurities. The spinel reflections exhibit a smooth transition to lower angles corresponding to a linear increase in lattice parameter as Ti content increases and the $CuTi_xCr_{2-x}S_4$ solid solution series approaches the $CuTi_2S_4$ end member. Elemental mapping of $CuTi_{1.5}Cr_{0.5}S_4$ shows a homogeneous distribution of Ti and Cr throughout the particles, confirming the successful preparation of a phase-pure solid solution (Figure 2b).

To prepare available spinel *A* sites for Mg^{2+} insertion, the copper ions in the spinel framework must be removed. Copper ions can be completely removed from $CuTi_2S_4$ after a 3-day

https://doi.org/10.1021/acsmaterialslett.1c00308
ACS Materials Lett. 2021, 3, 1213−1220

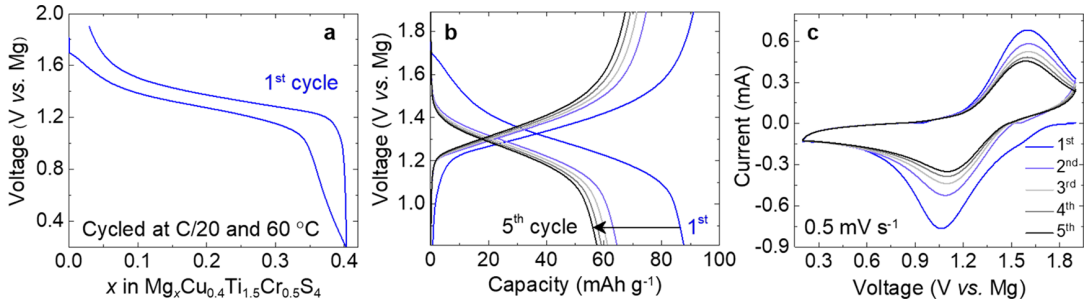

Figure 3. Electrochemical performance of $Cu_{0.4}Ti_{1.5}Cr_{0.5}S_4$||Mg cells at 60 °C using APC in THF as the electrolyte. (a) Galvanostatic cycling at a C/20 rate, (b) discharge/charge profiles of the first five cycles, and (c) cyclic voltammetry measured at a scan rate of 0.5 mV·s^{-1}. In each panel, the first cycle is shown in blue, and panels b and c share the same legend for the cycle number.

chemical oxidation using bromine in acetonitrile; however, additional time is required when Cr is present, which may parallel the difficulty of Mg^{2+} extraction from $MgCr_2S_4$. Relative to the pristine material, there is no discernible difference in the diffraction pattern of $CuTi_{1.5}Cr_{0.5}S_4$ after a 3-day oxidation, but there is evidence of copper removal after 1 week (Figure S4). As copper is removed, the intensity of the (111) reflection increases and the spinel peaks shift to the right, suggesting contraction of the spinel lattice. Complete copper removal is typically accompanied by the disappearance of the (220) and (422) reflections,[24] but residual intensity remains even in a $Cu_yTi_{1.5}Cr_{0.5}S_4$ sample oxidized for 2 weeks. The presence of these reflections indicates that copper has only partially been removed so that residual copper remains in the *A* sites. However, additional oxidation time produced no further changes in the diffraction pattern. Elemental analysis of oxidized samples showed that the extent of copper removal strongly depends on the relative amount of chromium in the material, where increased chromium content is accompanied by significant copper retention (Figure S5). After oxidation, the Ti-rich material was the only sample that achieved significant copper extraction with an average composition of $Cu_{0.44(5)}Ti_{1.5}Cr_{0.5}S_4$. To serve as a viable cathode material, the spinel framework needs to have empty *A* sites available for Mg^{2+} intercalation; therefore, this Ti-rich material was the only sample further investigated electrochemically.

The electrochemical behavior of $Cu_{0.4}Ti_{1.5}Cr_{0.5}S_4$||Mg coin cells was measured at 60 °C using APC in THF as the electrolyte. Figure 3a shows that 0.4 mol of Mg^{2+} can be inserted into the electrode material at an average discharge potential of 1.3 V, slightly higher than that of Ti_2S_4 (1.2 V).[22] The sloping nature of the discharge curve from 1.6 to 1.2 V demonstrates that a $Mg_xCu_{0.4}Ti_{1.5}Cr_{0.5}S_4$ solid solution forms as Mg^{2+} ions intercalate into the framework. The limited capacity of $Cu_{0.4}Ti_{1.5}Cr_{0.5}S_4$ relative to Ti_2S_4 (90 mAh·g^{-1} vs 200 mAh·g^{-1}) is a direct consequence of the residual Cu, which results in an increased formula weight and diminished number of *A* sites available for Mg^{2+} ions. Like previously reported thiospinel cathodes, an irreversible capacity loss occurs after the first cycle, which indicates that some of the inserted Mg^{2+} is trapped within the spinel framework (Figure 3b).[22,24] After this initial capacity loss, relatively stable cycling was achieved, but a gradual capacity fade was also observed. It is possible that this continued capacity loss is a result of the dissolution of active material on charge, as was observed for $MgCr_2S_4$. Cyclic voltammetry (CV) of the first five cycles of $Mg_xCu_{0.4}Ti_{1.5}Cr_{0.5}S_4$ shows only one oxidation peak located at 1.6 V vs Mg corresponding to the Ti^{3+}/Ti^{4+} redox couple with no evidence of Cr redox activity (Figure 3c). Thus, apart from the lower capacity, the electrochemical performance of $Cu_{0.4}Ti_{1.5}Cr_{0.5}S_4$ closely resembles that of Ti_2S_4. Taken together, the studies of $MgCr_2S_4$ and $Mg_xCu_{0.4}Ti_{1.5}Cr_{0.5}S_4$ point to an inactivity of Cr redox in thiospinels.

The identification of $MgCr_2S_4$ thiospinel as a potential cathode for Mg batteries resulted from a computational screening where this material was calculated to have desirable thermodynamic stability, voltage, capacity, and Mg^{2+} migration barriers.[20] The inaccessibility of Cr redox observed experimentally points to an insufficiency in these screening criteria and demands an investigation of the electronic structure of these materials. The calculated density of states (DOS) for MgM_2S_4 thiospinels (*M* = Ti, V, Cr) are shown in Figure 4 and

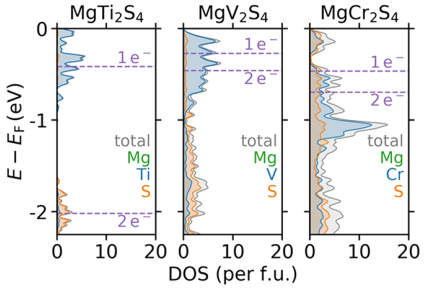

Figure 4. Electronic structure of fully discharged Mg thiospinels (transition metal varies from Ti to V to Cr moving left to right). The density of states (DOS) is normalized per MgB_2S_4 formula unit (f.u.), and the energy (*E*) is shown with respect to the Fermi energy (E_F) of each compound. The total DOS along with the element-projected DOS for the alkali (Mg), transition metal (*B*), and anion (S) are shown in gray, green, blue, and orange, respectively. Dashed purple lines represent the energy level at which 1 e$^-$ and 2 e$^-$ below E_F are accounted for in the DOS. The line for the 1 e$^-$ (2 e$^-$) nominally refers to the depth in energy that must be oxidized to remove 50% (100%) of the Mg.

reveal the effect of transition metal substitutions on the energy levels of redox couples. For these thiospinels, as the transition metal moves right in the periodic table (from Ti to V to Cr), the energy level of occupied S *p* states shifts up relative to the energy level of occupied transition metal *d* states. Here, we propose that this relative shift of anion vs cation states can be quantified and used as a descriptor to help predict the propensity for anion vs cation redox upon charge. This theoretical analysis can be used as a rapid screening protocol to better evaluate future materials in the hunt for novel Mg cathodes.

https://doi.org/10.1021/acsmaterialslett.1c00308
ACS Materials Lett. 2021, 3, 1213−1220

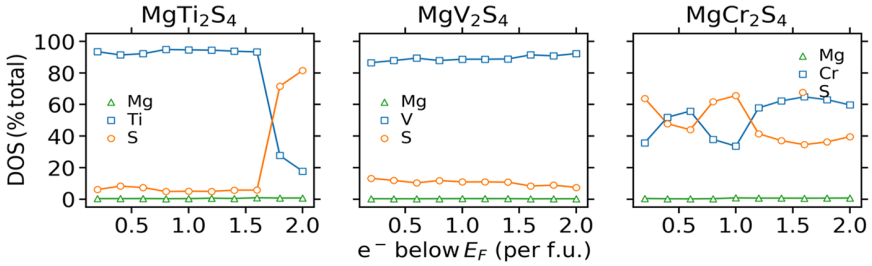

Figure 5. Tendency for oxidation of each ion in Mg thiospinels where the transition metal in the spinel is varied from Ti to V to Cr moving from left to right.

By integrating the DOS and assuming a rigid electronic structure upon alkali removal, we can quantify the relative prevalence of each ion's electronic states as we move down in energy from the Fermi level, E_F. The complete charge of these materials requires the removal of 2 e^- per formula unit. In Figure 5, we compare the quantity of states present for each ion within these first 2 e^- below E_F. Each data point accounts for the DOS belonging to the energy window corresponding with the previous 0.2 e^- of oxidation. That is, the data point at 1.0 e^- corresponds with each element's fraction of the total DOS over the energy window corresponding with 0.8 e^- to 1.0 e^- (0.4 to 0.5 Mg^{2+} removed per MgB_2S_4 spinel formula unit). It should be noted that this approach does not distinguish between covalency contributions of the anion to the metal states[32] or direct hole formation on the anion,[33] but it does give an indication of how much the anion states contribute to the oxidation process. Precisely how the anion states respond to oxidation is partly determined by the structure of the material(s) in question, for example, whether it can accommodate anion−anion dimers.[34] In this work, we focus only on the electronic structure of the thiospinel frameworks. In $MgTi_2S_4$, up to 1.6 e^-, Ti accounts for more than 90% of the DOS while S is only about 5% indicating that oxidation is mainly provided by Ti. Oxidation of metal states lowers their energy, and the more pronounced contribution of S in the last 0.4 e^- (0.2 Mg^{2+}) of oxidation is suggestive of strong Ti−S hybridization or possible sulfur oxidation. The latter interpretation would be consistent with our previous experimental report on $MgTi_2S_4$ that exhibited Mg^{2+} trapping after the first discharge so that inserted cations could not be completely extracted.[22] Only 80% of the theoretical capacity was achieved during discharge of $Mg_xTi_2S_4$ due to the sharp increase in the activation energy for diffusion at high Mg^{2+} concentration. While kinetic factors may also play a role in preventing complete demagnesiation, our analysis of the Ti-thiospinel electronic structure suggests that thermodynamics contributes to the incomplete Mg^{2+} extraction that was observed.

The inaccessible nature of the $Cr^{3+/4+}$ redox couple in the Cr-thiospinel system is consistent with previous investigations of chromium sulfide materials, as Cr^{4+} is typically not a stable cation in the presence of sulfur.[35−37] In contrast, the $Ti^{3+/4+}$ redox couple is accessible because Ti *d* levels sit well above the valence band built from S *s* and *p* states and are thus positioned high enough to stabilize the 4+ oxidation state. However, moving to the right of the periodic table (from Ti to V to Cr), the transition metal states move down relative to the S levels so that they fall into the *sp* band as shown in Figure 4. Because the states near E_F in fully discharged $MgCr_2S_4$ are dominated by S (Figure 5), initial charging of this material would require S oxidation to extract Mg^{2+} ions. Based on our inability to extract Mg^{2+} from $MgCr_2S_4$ and this electronic structure analysis, we speculate that initial charging leads to the formation of S holes that destabilize the spinel and trigger decomposition of the framework. This electronic structure analysis suggests that thiospinels with V appear as a trade-off between Ti and Cr and may offer a higher voltage cathode material than $MgTi_2S_4$ that exhibits transition metal redox. Despite this promise, MgV_2S_4 may not viably serve as a Mg cathode due to the thermodynamic instability of its charged and discharged states.[20] Thus, it is critical to consider a wide variety of criteria when screening for potential candidates.

Overall, the electrochemical behavior of $MgTi_xCr_{2-x}S_4$ materials demonstrates that reversible cation (de)intercalation from the spinel framework requires a redox-active transition metal present in the spinel *B* site. Without the presence of a redox-active transition metal, (electro)chemical oxidation would require S oxidation through the formation of S holes. Such reversible anionic redox activity has been demonstrated in sodium chromium sulfide layered materials, as antisite defect formation allows for the formation of S-dimers to stabilize the electrode active material.[34,38] In a spinel, however, such dimerization is restricted and cation extraction from the *A* site enabled by anionic redox activity triggers the decomposition of the structure, possibly along with the formation of soluble polysulfide species. While it may be possible to achieve a high-capacity Mg cathode in a layered structure that operates on reversible anionic redox activity, such a material would not provide a sufficiently high energy density owing to its relatively low operating potential. It is vital to access the high voltage Cr redox couple. To date, this has been achieved only once in a sulfide, where XPS analysis of a $KCrS_2$ cathode material at various states of charge showed a continuous increase of Cr^{4+}/Cr^{3+} ratios and a simultaneous invariance of the peak features of sulfur as K^+ content decreased.[39] Thus, detailed investigations of this $KCrS_2$ material are needed in order to understand fundamental principles governing its charge storage mechanism and to understand how structure can be tailored to access the high voltage $Cr^{3+/4+}$ couple in the presence of sulfur.

■ CONCLUSIONS

Mg^{2+} ions cannot be extracted from $MgCr_2S_4$ because thiospinel frameworks only exhibit reversible electrochemistry when a redox-active transition metal is present in the *B* site, and Cr *d* levels are not high enough in energy (relative to S *p*) to stabilize the 4+ state. Without a redox-active *B* site metal, *A*-site extraction is enabled by anionic redox activity and the formation of S holes. Unlike layered structures, S-dimerization is restricted in the relatively rigid spinel framework. As a result, S oxidation triggers decomposition of the spinel and possible

https://doi.org/10.1021/acsmaterialslett.1c00308
ACS Materials Lett. 2021, 3, 1213−1220

dissolution of soluble polysulfide species. A layered framework—which provides lower activation energy for the formation of antisite defects and/or more available pathways for migration—could allow access to the high voltage Cr redox couple in a sulfide to allow for reversible Mg^{2+} (de)-intercalation. Design of such a Mg_xCrS_2 cathode material critically relies on a fundamental understanding of the electrochemical activity of $ACrS_2$ (A = Na, K, etc.) cathodes and how differences in their (electro)chemical structures enable various redox mechanisms to favor anionic and/or Cr activity.

EXPERIMENTAL SECTION

Material Synthesis. Nanosized $MgCr_2S_4$ was directly prepared using a recently reported metathesis reaction.[30] Micron-sized $CuTi_xCr_{2-x}S_4$ spinel solid solutions (x = 0, 0.5, 1, 1.5, or 2) were synthesized by mixing the elements in stoichiometric ratios and grinding with a mortar and pestle inside an Ar-filled glovebox. The resulting powders were pelletized, sealed in an evacuated quartz tube, and heated to 800 °C for 2 days after a 12 h hold at 500 °C. Copper was chemically extracted using bromine in acetonitrile, as described in our previous publication.[22] These room temperature oxidations were repeated multiple times for Cr-containing materials, until Cu could no longer be removed.

Material Characterization. X-ray diffraction (XRD) was carried out on a PANalytical Empyrean diffractometer with Cu Kα radiation. Material morphologies and elemental compositions were examined using a Zeiss field emission scanning electron microscope (SEM) equipped with an energy dispersive X-ray spectroscopy (EDX) detector. Samples were transferred to the instrument with minimal exposure to air and scans were collected at an accelerating voltage of 20 keV. *Ex situ* X-ray absorption spectroscopy (XAS) measurements were carried out in a transmission mode at room temperature using the beamline 20-BM at the Advanced Photon Source of the Argonne National Laboratory. The prepared XAS samples were sealed with polyimide tape (Kapton, DuPont) to prevent air exposure. The incident beam energy was selected using a Si (111) monochromator, and the beam intensity was reduced by 15% using a Rh-coated mirror to minimize high-order harmonics. A reference spectrum of Cr metal was collected simultaneously using pure Cr metal foil. The X-ray absorption near edge structure (XANES) data were analyzed using the Athena program, and the spectral energies were calibrated using the first inflection point in the spectra of Cr metal foil. XPS measurements were performed on a Thermo Scientific K-Alpha XPS System with a monochromatic Al Kα X-ray source in the Molecular Foundry at the Lawrence Berkeley National Laboratory. Both the noncycled (pristine sample) and postcharged films were transferred into the XPS system using a Thermo Scientific K-Alpha Vacuum Transfer Module to avoid air exposure then cleaned using monatomic Ar ion milling (1000 eV, high current mode, 15 s) to remove surface-absorbed C and O. The spectra of Cr 2p and S 2p were acquired with passing energy of 50 eV and a dwell time of 50 ms.

Electrochemical Studies. $MgCr_2S_4$ electrodes were prepared with a 7:2:1 weight ratio of active material, conductive carbon, and polytetrafluoroethylene (PTFE) binder. $Cu_{0.4}Ti_{1.5}Cr_{0.5}S_4$ electrodes were prepared with an 8:1:1 weight ratio of active material, conductive carbon (Super P), and polyvinylidene fluoride (PVDF, average Mw ≈ 534 000) inside an Ar-filled glovebox. The electrode slurry was ground in *N*-methyl-2-pyrrolidone (NMP, Sigma-Aldrich 99.5%) and cast on to Mo foil and dried at elevated temperature. Mg coin cells (2325) were assembled with a polished Mg metal counter electrode and an all-phenyl complex (APC) electrolyte with tetrahydrofuran (THF) as the solvent.[40] The electrochemistry of these cells was examined in galvanostatic mode using a VMP3 potentiostat/galvanostat (Biologic).

Computational Methods. Each compound was calculated in the 14-atom spinel ($Fd\bar{3}m$) unit cell (queried from the Materials Project database[41]) with density functional theory (DFT) using the Vienna Ab Initio Simulation Package (VASP)[42,43] and projector augmented wave (PAW) method.[44,45] The SCAN meta-GGA density functional[46] was used with a plane-wave energy cutoff of 520 eV and a Γ-centered Monkhorst−Pack k-point grid with $25|b_i|$ discretizations along each reciprocal lattice vector, b_i. All calculations were spin-polarized with high-spin ferromagnetic initial configurations and converged to 10^{-6} eV·atom^{-1} for electronic optimization and 10^{-2} eV·Å^{-1} for ionic optimization.

ASSOCIATED CONTENT

Supporting Information

The Supporting Information is available free of charge at https://pubs.acs.org/doi/10.1021/acsmaterialslett.1c00308.

Schematic of $MgCr_2S_4$ metathesis synthesis along with $Mg_xCr_2S_4$ charge capacity and EDX characterization; XRD and SEM-EDX characterizations of oxidized $Cu_yTi_{2-x}Cr_xS_4$ samples (PDF)

AUTHOR INFORMATION

Corresponding Authors

Linda F. Nazar − *Department of Chemistry and the Waterloo Institute for Nanotechnology, University of Waterloo, Waterloo, ON N2L 3G1, Canada;* orcid.org/0000-0002-3314-8197; Email: lfnazar@uwaterloo.ca

Gerbrand Ceder − *Department of Materials Science and Engineering, University of California, Berkeley, California 94720, United States; Materials Sciences Division, Lawrence Berkeley National Laboratory, Berkeley, California 94720, United States;* orcid.org/0000-0001-9275-3605; Email: gceder@berkeley.edu, gceder@lbl.gov

Authors

Lauren Blanc − *Department of Chemistry and the Waterloo Institute for Nanotechnology, University of Waterloo, Waterloo, ON N2L 3G1, Canada*

Christopher J. Bartel − *Department of Materials Science and Engineering, University of California, Berkeley, California 94720, United States;* orcid.org/0000-0002-5198-5036

Haegyeom Kim − *Materials Sciences Division, Lawrence Berkeley National Laboratory, Berkeley, California 94720, United States*

Yaosen Tian − *Department of Materials Science and Engineering, University of California, Berkeley, California 94720, United States*

Hyunchul Kim − *Materials Sciences Division, Lawrence Berkeley National Laboratory, Berkeley, California 94720, United States;* orcid.org/0000-0002-8006-9504

Akira Miura − *Faculty of Engineering, Hokkaido University, Sapporo 060-8628, Japan;* orcid.org/0000-0003-0388-9696

https://doi.org/10.1021/acsmaterialslett.1c00308
ACS Materials Lett. 2021, 3, 1213−1220

Complete contact information is available at:
https://pubs.acs.org/10.1021/acsmaterialslett.1c00308

Author Contributions

#L.B. and C.J.B. contributed equally to this work.

Notes

The authors declare no competing financial interest.

■ ACKNOWLEDGMENTS

This work was supported by the Joint Center for Energy Storage Research (JCESR), an Energy Innovation Hub funded by the U.S. Department of Energy (DOE), Office of Science, Basic Energy Sciences. L.F.N. gratefully acknowledges the Natural Sciences and Engineering Research Council of Canada (NSERC) for a Canada Research Chair and for funding through the NSERC Discovery Grants program. This work utilized high-performance computing resources through the National Energy Research Scientific Computing Center (NERSC), a U.S. Department of Energy Office of Science User Facility operated under Contract No. DE-AC02-05CH11231, and the Savio computational cluster resource provided by the Berkeley Research Computing program at the University of California, Berkeley (supported by the UC Berkeley Chancellor, Vice Chancellor for Research, and Chief Information Officer). Work at the Molecular Foundry was supported by the Office of Science, Office of Basic Energy Sciences, of the U.S. Department of Energy under Contract No. DE-AC02-05CH11231.

■ REFERENCES

(1) Armand, M.; Tarascon, J.-M. Building Better Batteries. *Nature* **2008**, *451*, 652−657.
(2) Thackeray, M. M.; Wolverton, C.; Isaacs, E. D. Electrical Energy Storage for Transportation—Approaching the Limits of, and Going beyond, Lithium-Ion Batteries. *Energy Environ. Sci.* **2012**, *5*, 7854−7863.
(3) Cabana, J.; Monconduit, L.; Larcher, D.; Palacín, M. R. Beyond Intercalation-Based Li-Ion Batteries: The State of the Art and Challenges of Electrode Materials Reacting Through Conversion Reactions. *Adv. Mater.* **2010**, *22*, E170−E192.
(4) El Kharbachi, A.; Zavorotynska, O.; Latroche, M.; Cuevas, F.; Yartys, V.; Fichtner, M. Exploits, Advances and Challenges Benefiting beyond Li-Ion Battery Technologies. *J. Alloys Compd.* **2020**, *817*, 153261.
(5) Shah, R.; Mittal, V.; Matsil, E.; Rosenkranz, A. Magnesium-Ion Batteries for Electric Vehicles: Current Trends and Future Perspectives. *Adv. Mech. Eng.* **2021**, *13*, 168781402110033.
(6) Canepa, P.; Sai Gautam, G.; Hannah, D. C.; Malik, R.; Liu, M.; Gallagher, K. G.; Persson, K. A.; Ceder, G. Odyssey of Multivalent Cathode Materials: Open Questions and Future Challenges. *Chem. Rev.* **2017**, *117*, 4287−4341.
(7) Yoo, H. D.; Shterenberg, I.; Gofer, Y.; Gershinsky, G.; Pour, N.; Aurbach, D. Mg Rechargeable Batteries: An On-Going Challenge. *Energy Environ. Sci.* **2013**, *6*, 2265−2279.
(8) Muldoon, J.; Bucur, C. B.; Gregory, T. Quest for Nonaqueous Multivalent Secondary Batteries: Magnesium and Beyond. *Chem. Rev.* **2014**, *114*, 11683−11720.
(9) Muldoon, J.; Bucur, C. B.; Gregory, T. Fervent Hype behind Magnesium Batteries: An Open Call to Synthetic Chemists-Electrolytes and Cathodes Needed. *Angew. Chem., Int. Ed.* **2017**, *56*, 12064−12084.
(10) Bonnick, P.; Muldoon, J. A Trip to Oz and a Peak Behind the Curtain of Magnesium Batteries. *Adv. Funct. Mater.* **2020**, *30*, 1910510.
(11) Matsui, M. Study on Electrochemically Deposited Mg Metal. *J. Power Sources* **2011**, *196*, 7048−7055.
(12) Li, M.; Lu, J.; Ji, X.; Li, Y.; Shao, Y.; Chen, Z.; Zhong, C.; Amine, K. Design Strategies for Nonaqueous Multivalent-Ion and Monovalent-Ion Battery Anodes. *Nat. Rev. Mater.* **2020**, *5*, 276−294.
(13) Bonnick, P.; Sun, X.; Lau, K.-C.; Liao, C.; Nazar, L. F. Monovalent versus Divalent Cation Diffusion in Thiospinel Ti_2S_4. *J. Phys. Chem. Lett.* **2017**, *8*, 2253−2257.
(14) Ling, C.; Zhang, R.; Arthur, T. S.; Mizuno, F. How General Is the Conversion Reaction in Mg Battery Cathode: A Case Study of the Magnesiation of α-MnO_2. *Chem. Mater.* **2015**, *27*, 5799−5807.
(15) Ling, C.; Zhang, R.; Mizuno, F. Quantitatively Predict the Potential of MnO_2 Polymorphs as Magnesium Battery Cathodes. *ACS Appl. Mater. Interfaces* **2016**, *8*, 4508−4515.
(16) Tchitchekova, D. S.; Monti, D.; Johansson, P.; Bardé, F.; Randon-Vitanova, A.; Palacín, M. R.; Ponrouch, A. On the Reliability of Half-Cell Tests for Monovalent (Li^+, Na^+) and Divalent (Mg^{2+}, Ca^{2+}) Cation Based Batteries. *J. Electrochem. Soc.* **2017**, *164*, A1384.
(17) Kundu, D.; Vajargah, S. H.; Wan, L.; Adams, B.; Prendergast, D.; Nazar, L. F. Aqueous vs. Nonaqueous Zn-Ion Batteries: Consequences of the Desolvation Penalty at the Interface. *Energy Environ. Sci.* **2018**, *11*, 881−892.
(18) Lipson, A. L.; Han, S.-D.; Pan, B.; See, K. A.; Gewirth, A. A.; Liao, C.; Vaughey, J. T.; Ingram, B. J. Practical Stability Limits of Magnesium Electrolytes. *J. Electrochem. Soc.* **2016**, *163*, A2253−A2257.
(19) Zhang, R.; Ling, C. Unveil the Chemistry of Olivine $FePO_4$ as Magnesium Battery Cathode. *ACS Appl. Mater. Interfaces* **2016**, *8*, 18018−18026.
(20) Liu, M.; Jain, A.; Rong, Z.; Qu, X.; Canepa, P.; Malik, R.; Ceder, G.; Persson, K. A. Evaluation of Sulfur Spinel Compounds for Multivalent Battery Cathode Applications. *Energy Environ. Sci.* **2016**, *9*, 3201−3209.
(21) Aurbach, D.; Lu, Z.; Schechter, A.; Gofer, Y.; Gizbar, H.; Turgeman, R.; Cohen, Y.; Moshkovich, M.; Levi, E. Prototype Systems for Rechargeable Magnesium Batteries. *Nature* **2000**, *407*, 724−727.
(22) Sun, X.; Bonnick, P.; Duffort, V.; Liu, M.; Rong, Z.; Persson, K. A.; Ceder, G.; Nazar, L. F. A High Capacity Thiospinel Cathode for Mg Batteries. *Energy Environ. Sci.* **2016**, *9*, 2273−2277.
(23) Sun, X.; Bonnick, P.; Nazar, L. F. Layered TiS_2 Positive Electrode for Mg Batteries. *ACS Energy Lett.* **2016**, *1*, 297−301.
(24) Bonnick, P.; Blanc, L.; Vajargah, S. H.; Lee, C.-W.; Sun, X.; Balasubramanian, M.; Nazar, L. F. Insights into Mg^{2+} Intercalation in a Zero-Strain Material: Thiospinel $Mg_xZr_2S_4$. *Chem. Mater.* **2018**, *30*, 4683−4693.
(25) Liu, M.; Rong, Z.; Malik, R.; Canepa, P.; Jain, A.; Ceder, G.; Persson, K. A. Spinel Compounds as Multivalent Battery Cathodes: A Systematic Evaluation Based on Ab Initio Calculations. *Energy Environ. Sci.* **2015**, *8*, 964−974.
(26) Rong, Z.; Malik, R.; Canepa, P.; Sai Gautam, G.; Liu, M.; Jain, A.; Persson, K.; Ceder, G. Materials Design Rules for Multivalent Ion Mobility in Intercalation Structures. *Chem. Mater.* **2015**, *27*, 6016−6021.
(27) Parajuli, P.; Park, H.; Kwon, B. J.; Guo, J.; Key, B.; Vaughey, J. T.; Zapol, P.; Klie, R. F. Direct Observation of Electron Beam-Induced Phase Transition in $MgCrMnO_4$. *Chem. Mater.* **2020**, *32*, 10456−10462.
(28) Shimokawa, K.; Ichitsubo, T. Spinel−Rocksalt Transition as a Key Cathode Reaction toward High-Energy-Density Magnesium Rechargeable Batteries. *Curr. Opin. Electrochem.* **2020**, *21*, 93−99.
(29) Wustrow, A.; Key, B.; Phillips, P. J.; Sa, N.; Lipton, A. S.; Klie, R. F.; Vaughey, J. T.; Poeppelmeier, K. R. Synthesis and Characterization of $MgCr_2S_4$ Thiospinel as a Potential Magnesium Cathode. *Inorg. Chem.* **2018**, *57*, 8634−8638.
(30) Miura, A.; Ito, H.; Bartel, C. J.; Sun, W.; Rosero-Navarro, N. C.; Tadanaga, K.; Nakata, H.; Maeda, K.; Ceder, G. Selective Metathesis Synthesis of $MgCr_2S_4$ by Control of Thermodynamic Driving Forces. *Mater. Horiz.* **2020**, *7*, 1310.

(31) Blanc, L. E.; Sun, X.; Shyamsunder, A.; Duffort, V.; Nazar, L. F. Direct Nano-Synthesis Methods Notably Benefit Mg-Battery Cathode Performance. *Small Methods* **2020**, *4*, 2000029.
(32) Aydinol, M. K.; Kohan, A. F.; Ceder, G.; Cho, K.; Joannopoulos, J. Ab Initio Study of Lithium Intercalation in Metal Oxides and Metal Dichalcogenides. *Phys. Rev. B: Condens. Matter Mater. Phys.* **1997**, *56*, 1354−1365.
(33) Seo, D.-H.; Lee, J.; Urban, A.; Malik, R.; Kang, S.; Ceder, G. The Structural and Chemical Origin of the Oxygen Redox Activity in Layered and Cation-Disordered Li-Excess Cathode Materials. *Nat. Chem.* **2016**, *8*, 692−697.
(34) Wang, T.; Ren, G.-X.; Shadike, Z.; Yue, J.-L.; Cao, M.-H.; Zhang, J.-N.; Chen, M.-W.; Yang, X.-Q.; Bak, S.-M.; Northrup, P.; Liu, P.; Liu, X.-S.; Fu, Z.-W. Anionic Redox Reaction in Layered $NaCr_{2/3}Ti_{1/3}S_2$ through Electron Holes Formation and Dimerization of S−S. *Nat. Commun.* **2019**, *10*, 1−12.
(35) Rouxel, J. Anion−Cation Redox Competition and the Formation of New Compounds in Highly Covalent Systems. *Chem. - Eur. J.* **1996**, *2*, 1053−1059.
(36) Rouxel, J.; Tournoux, M. Chimie Douce with Solid Precursors, Past and Present. *Solid State Ionics* **1996**, *84*, 141−149.
(37) Bodenez, V.; Dupont, L.; Morcrette, M.; Surcin, C.; Murphy, D. W.; Tarascon, J.-M. Copper Extrusion/Reinjection in Cu-Based Thiospinels by Electrochemical and Chemical Routes. *Chem. Mater.* **2006**, *18*, 4278−4287.
(38) Shadike, Z.; Zhou, Y.-N.; Chen, L.-L.; Wu, Q.; Yue, J.-L.; Zhang, N.; Yang, X.-Q.; Gu, L.; Liu, X.-S.; Shi, S.-Q.; Fu, Z.-W. Antisite Occupation Induced Single Anionic Redox Chemistry and Structural Stabilization of Layered Sodium Chromium Sulfide. *Nat. Commun.* **2017**, *8*, 566.
(39) Naveen, N.; Park, W. B.; Singh, S. P.; Han, S. C.; Ahn, D.; Sohn, K.-S.; Pyo, M. $KCrS_2$ Cathode with Considerable Cyclability and High Rate Performance: The First K^+ Stoichiometric Layered Compound for Potassium-Ion Batteries. *Small* **2018**, *14*, 1803495.
(40) Mizrahi, O.; Amir, N.; Pollak, E.; Chusid, O.; Marks, V.; Gottlieb, H.; Larush, L.; Zinigrad, E.; Aurbach, D. Electrolyte Solutions with a Wide Electrochemical Window for Rechargeable Magnesium Batteries. *J. Electrochem. Soc.* **2008**, *155*, A103−A109.
(41) Jain, A.; Ong, S. P.; Hautier, G.; Chen, W.; Richards, W. D.; Dacek, S.; Cholia, S.; Gunter, D.; Skinner, D.; Ceder, G.; Persson, K. A. Commentary: The Materials Project: A Materials Genome Approach to Accelerating Materials Innovation. *APL Mater.* **2013**, *1*, No. 011002.
(42) Kresse, G.; Furthmüller, J. Efficient Iterative Schemes for Ab Initio Total-Energy Calculations Using a Plane-Wave Basis Set. *Phys. Rev. B: Condens. Matter Mater. Phys.* **1996**, *54*, 11169−11186.
(43) Kresse, G.; Furthmüller, J. Efficiency of Ab-Initio Total Energy Calculations for Metals and Semiconductors Using a Plane-Wave Basis Set. *Comput. Mater. Sci.* **1996**, *6*, 15−50.
(44) Kresse, G.; Joubert, D. From Ultrasoft Pseudopotentials to the Projector Augmented-Wave Method. *Phys. Rev. B: Condens. Matter Mater. Phys.* **1999**, *59*, 1758−1775.
(45) Blöchl, P. E. Projector Augmented-Wave Method. *Phys. Rev. B: Condens. Matter Mater. Phys.* **1994**, *50*, 17953−17979.
(46) Sun, J.; Ruzsinszky, A.; Perdew, J. P. Strongly Constrained and Appropriately Normed Semilocal Density Functional. *Phys. Rev. Lett.* **2015**, *115*, No. 036402.

https://doi.org/10.1021/acsmaterialslett.1c00308
ACS Materials Lett. 2021, 3, 1213−1220